addition of 10 mL of hexane, and filtering to give **20** as an orange-red solid. Evaporation of the mother liquor and treatment of the residue with CH_2Cl_2/hexane gave an additional quantity of **20** (105 mg total, 68%): ^1H NMR (500 MHz, acetone-d_6) δ 11.04 (d, J = 12.7 Hz, μ-CH), 4.89 (s, 10 H, C_5H_5), 4.33 (d, J = 12.7 Hz, μ-CHC*H*), 4.28 (qd, J = 7.1, 10.8 Hz, C*H*HCH$_3$), 4.24 (qd, J = 7.1, 10.8 Hz, CH*H*CH$_3$) 1.30 (t, 6 H, J = 7.1 Hz, CHHC*H*$_3$); $^{13}C\{^1H\}$ NMR (125.76 MHz, acetone-d_6) δ 270.2 (μ-CO), 213.3 (CO), 169.9 (*C*OCH$_2$CH$_3$), 158.8 (μ-CHR), 88.7 (C_5H_5), 74.3 (μ-CH*C*H), 61.4 (*C*H$_2$CH$_3$), 14.6 (CH$_2$*C*H$_3$); IR (CH_2Cl_2) 1995 (s), 1950 (w), 1795 (m), 1750 (w), 1730 (w), 1650 (w) cm^{-1}; HRMS calcd for M – CO $C_{20}H_{22}Fe_2O_6$ 470.0114, found 470.0088.

Acknowledgment. Support from the Department of Energy, Division of Basic Energy Science, and the National Science Foundation is gratefully acknowledged. M.C. thanks the Science and Engineering Research Council (U.K.) for a NATO postdoctoral fellowship.

Registry No. 1, 82660-13-7; 2, 79839-80-8; 3, 83681-74-7; 4a, 83730-01-2; 4b, 83681-78-1; 6 (isomer 1), 112172-84-6; 6 (isomer 2), 112318-69-1; 7, 93842-65-0; 9-PF_6, 112172-86-8; 9-BF_4, 112318-70-4; 10, 112172-85-7; 11 (isomer 1), 75811-60-8; 11 (isomer 2), 112318-71-5; 12, 112172-87-9; 13, 112172-88-0; 14, 112172-89-1; 15, 112172-90-4; 16, 112172-91-5; 17, 112172-92-6; 18, 112172-93-7; 19, 112172-94-8; 20, 112172-95-9; $[(C_5H_5)(CO)Fe]_2(\mu\text{-}CO)_2$, 12154-95-9; $(C_5H_5)Fe(CO)_2Br$, 12078-20-5; $[(C_5H_5)(CO)Fe]_2(\mu\text{-}CO)[\mu\text{-}CHCH{=}C(CH_3)_2]$, 112172-96-0; $Ph_2C{=}NH$, 1013-88-3; $Li(C_6H_5CuCN)$, 41742-64-7; $(C_2H_5)_4N^+HFe(CO)_4^-$, 25879-01-0; diisopropylethylamine, 7087-68-5; acetone, 67-64-1; cyclohexanone, 108-94-1; 2-butanone, 78-93-3; 4-methyl-2-pentanone, 108-10-1; 2,4-pentanedione, 626-96-0; 5,5-dimethyl-1,3-cyclohexanedione, 126-81-8; ethyl acetoacetate, 141-97-9; sodium diethyl malonate, 51923-79-6.

Modeling Fischer–Tropsch Chemistry: The Thermochemistry and Insertion Kinetics of ClRuH(CH_2)

Emily A. Carter† and William A. Goddard III*

Arthur Amos Noyes Laboratory of Chemical Physics, California Institute of Technology,‡ Pasadena, California 91125

Received July 10, 1987

The insertions of metal-bound CH_x into M–H and M–CH_3 bonds have been proposed as the chain initiation and propagation steps, respectively, in the Fischer–Tropsch reductive polymerization of CO to form alkanes. As a model for this important elementary reaction, we have examined the properties and migratory insertion reactivity of a prototypical coordinatively saturated complex ClRuH(CH_2) using ab initio methods (generalized valence bond + configuration interaction). The Ru=CH_2 double bond is covalent, with D_e(Ru=C) = 84.7 kcal/mol. The optimum geometry has the CH_2 plane perpendicular to the ClRuH plane, with a rotational barrier of ≥13.6 kcal/mol. The lowest energy conformer of the singlet state of ClRuH(CH_2) has an in-plane π bond, which facilitates the insertion of the CH_2 ligand into the adjacent Ru–H bond. Using analytic gradient techniques combined with GVB-MCSCF wave functions to find the minimum energy pathway, we find that the insertion proceeds with a moderate barrier (11.5 kcal/mol) and is exothermic by 7.1 kcal/mol. From a thermodynamic cycle designed to probe basis set and electron correlation deficiencies, we estimate an actual barrier to insertion of 10.9 ± 1.7 kcal/mol and an exothermicity of 10.5 ± 1.0 kcal/mol.

I. Introduction

Ruthenium complexes containing hydrido, alkyl, alkylidene, and alkylidyne ligands have been proposed as intermediates in metal-catalyzed C–H and C–C bond-forming processes.[1-3]

In homogeneous reactions, both CH_2 insertion into M–H and M–R bonds to make new metal alkyls[1]

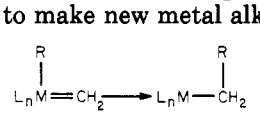

(1)

and intramolecular alkylidene coupling in binuclear Ru systems to make olefins

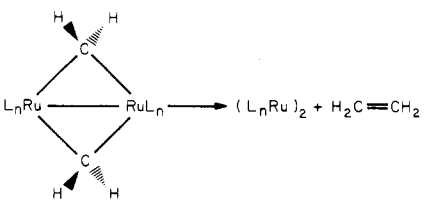

(2)

have been observed.[2] Catalytic reduction of CO to methanol, ethanol, and ethylene glycol by soluble Ru complexes have also been observed (eq 3).[3]

$$H_2 + CO \xrightarrow{Ru_3(CO)_{12}} CH_3OH + C_2H_5OH + HOCH_2CH_2OH \quad (3)$$

† Present address: Department of Chemistry and Biochemistry, Campus Box 215, University of Colorado, Boulder, CO 80309.

‡ Contribution No. 7583.

(1) (a) Cooper, N. J.; Green, M. L. H. *J. Chem. Soc., Dalton Trans.* **1979**, 1121. (b) Hayes, J. C.; Pearson, G. D. N.; Cooper, N. J. *J. Am. Chem. Soc.* **1981**, *103*, 4648–4650. (c) Thorn, D. L.; Tulip, T. H. *Ibid.* 5984–5986. (d) Canestrari, M.; Green, M. L. H. *J. Chem. Soc., Dalton Trans.* **1982**, 1789. (e) Isobe, K.; Andrews, D. G.; Mann, B. E.; Maitlis, P. M. *J. Chem. Soc., Chem. Commun.* **1981**, 809. (f) Thorn, D. L.; Tulip, T. H. *Organometallics* **1982**, *1*, 1580. (g) Hayes, J. C.; Cooper, N. J. *J. Am. Chem. Soc.* **1982**, *104*, 5570. (h) Kletzin, H.; Werner, H.; Serhadli, O.; Ziegler, M. L. *Angew. Chem. Int. Ed. Engl.* **1983**, *22*, 46. (i) Jernakoff, P.; Cooper, N. J. *J. Am. Chem. Soc.* **1984**, *106*, 3026. (j) Jernakoff, P.; Cooper, N. J. *Organometallics* **1986**, *5*, 747. (k) Thorn, D. L. *Ibid.* 1897.

(2) (a) Cooke, M.; Davies, D. L.; Guerchais, J. E.; Knox, S. A. R.; Mead, K. A.; Roué, J.; Woodward, P. *J. Chem. Soc., Chem. Commun.* **1981**, 862. (b) Herrmann, W. A. *Adv. Organomet. Chem.* **1981**, *20*, 249. Other C–C couplings at μ-CH_2Ru_2 centers include: Colborn, R. E.; Dyke, A. F.; Knox, S. A. R.; MacPherson, K. A.; Orpen, A. G. *J. Organomet. Chem.* **1982**, *239*, C15. Adams, P. Q.; Davies, D. L.; Dyke, A. F.; Knox, S. A. R.; Mead, K. A.; Woodward, P. *J. Chem. Soc., Chem. Commun.* **1983**, 222.

(3) (a) Bradley, J. S. *J. Am. Chem. Soc.* **1979**, *101*, 7419. (b) Dombek, B. D. *Ibid.* **1980**, *102*, 6855. (c) Daroda, R. J.; Blackborrow, J. R.; Wilkinson, G. *J. Chem. Soc., Chem. Commun.* **1980**, 101. (d) Knifton, J. R. *Ibid.* **1981**, 188. (e) Warren, B. K.; Dombek, B. D. *J. Catal.* **1983**, *79*, 334.

0276-7333/88/2307-0675$01.50/0

In the heterogeneous Fischer–Tropsch (FT) synthesis of hydrocarbons from CO and H_2, the insertions of metal-bound CH_x fragments into metal–hydrogen and metal–alkyl bonds (eq 4) are thought to be responsible for the chain initiation and growth steps of the FT reaction.[4] The

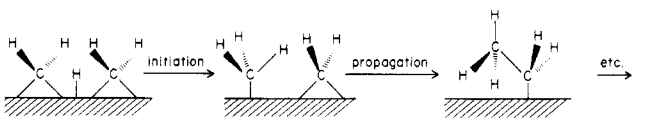

(4)

most active undoped catalyst is Ru metal, which readily produces high molecular weight polymethylenes.[5] The mechanism shown in (4) is particularly applicable to Ru catalysts since polymethylene may be produced simply through repeated CH_2 insertions into a growing alkyl chain. While methylene on the clean Ru(001) surface has been observed in bridging coordination sites at low temperature,[6] the actual insertion step of (4) may well require both reacting species to be coordinated to the same metal atom. Indeed Thorn and Tulip[1c,f] have provided evidence for both H and CH_3 migration to CH_2 at an Ir(I) center (eq 5), while

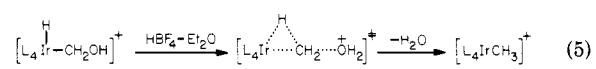

(5)

Cooper,[1a,b,g,i,j] Maitlis,[1e] and Werner[1h] have proposed methyl methylidene metal complexes as intermediates during dimethyl rearrangements to olefin hydrides (subsequent to hydrogen abstraction) (eq 6). These studies suggest

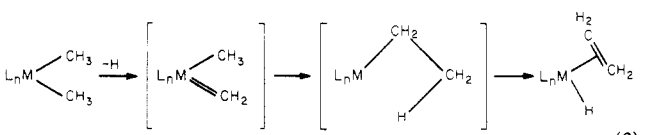

(6)

that both chain initiation and growth may be achieved at a single metal center.

In order to study the energetics and orbital requirements for such methylidene insertion processes, we have examined the reaction pathway (7).

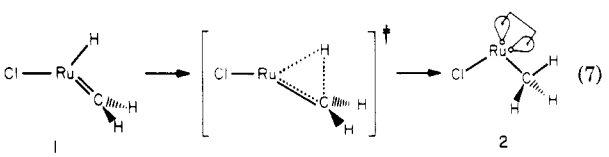

(7)

1 2

In the following discussions, it will be useful to follow the generalized valence bond (GVB) convention of oxidation states (based on the results of numerous calculations).[7] We start with the metal in a low-lying state of the *neutral* atom, e.g., s^1d^7 for Ru, s^2d^6 for Fe or Os. An electron-withdrawing ligand such as Cp (η^5-C_5H_5) or Cl is considered to oxidize the metal center by one unit. However, this electron must come from an s orbital (i.e., an easily ionized valence electron), and hence only up to a maximum of two units of charge can be ionized. Any remaining metal valence d orbitals that are singly occupied can form covalent bonds to less electronegative ligands such as alkyl, aryl, or hydrogen (or oxo). Donor ligands such as phosphine involve donation into empty metal valence orbitals (d, s, or p). The maximum number of metal orbitals used in all bonds is nine, allowing up to 18 electrons to surround the metal center. These bonding rules consider that Cl and Cp will form ionic bonds, π-aryls, phosphines, and CO will make donor bonds, and open-shell ligands such as R•, :CH_2, H•, and •NO will form covalent bonds to unpaired metal d electrons.

In the GVB description of **1**, we start with s^1d^7 Ru(0), but Cl removes the s electron to yield d^7 Ru(I). With a d^7 valence electron configuration, we can occupy the five d orbitals as

2 2 1 1 1 (quartet)

or as

2 2 2 1 0 (doublet)

Using the quartet configuration, we can form a double bond to CH_2 and a single bond to H, leading to an overall singlet state. At this point we have used only six metal orbitals (the s and five d). Replacing Cl^- with Cp^- requires two additional orbitals (for two additional donor bonds from Cp^-) and adding, e.g., a phosphine ligand uses one additional metal orbital for a total of nine.

Thus, the singlet state of $ClRu(CH_2)H$ (**1**) is a model for the 18-electron, coordinatively saturated complex $Cp(PR_3)Ru(R)(CH_2)$, in which the Cp and PR_3 groups are mimicked by the Cl and the low-spin state of **1** (the metal must be low spin so that PR_3 and Cp^- have four empty metal orbitals to donate into). Similarly, $[(C_6Me_6)(PPh_3)Ru(CH_3)(CH_2)]^+$ (**3**) is another complex for which low-spin **1** serves as a prototype, where the phosphine and the π-aryl group again force the metal to a low-spin state in order to have empty orbitals available for ligand donation and where the positive charge is mimicked by the chlorine ligand in **1**. Complex **3** has been postulated as an intermediate in the isomerization of a ruthenium dimethyl complex to a ruthenium ethylene hydride via the insertion of CH_2 into an adjacent Ru–CH_3 bond.[1h]

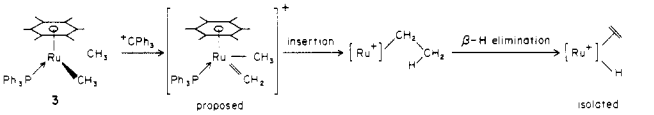

(8)

While CH_2 insertions into adjacent M–H(R) bonds have been observed indirectly for a number of homogeneous organometallic systems,[1] direct observation has eluded researchers until very recently. Magnetization transfer experiments of Bercaw and co-workers[8] directly directly monitored the insertion of CH_2 into the Ta–H bond of **4** above room temperature, yielding the 16-electron complex **5**.

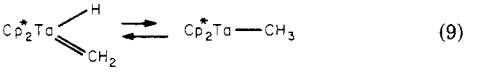

(9)

4 5

In the GVB description of **4**, we start with ground state s^2d^3 Ta(0) and let each Cp oxidize one s electron to yield a d^3 configuration for Ta(II): 1 1 1 0 0. This allows for the formation of a covalent double bond to CH_2 and a covalent single bond to H. Considering two additional donor bonds from each of the Cp π systems accounts for

(4) (a) Biloen, P.; Sachtler, W. M. H. *Adv. Catal.* **1981**, *30*, 165. (b) Brady, R. C., III; Pettit, R. *J. Am. Chem. Soc.* **1980**, *102*, 6181. (c) *Ibid.* **1981**, *103*, 1287. (d) Baker, J. A.; Bell, A. T. *J. Catal.* **1982**, *78*, 165.

(5) (a) Anderson, R. B. In *Catalysis: Hydrocarbon Synthesis, Hydrogenation, and Cyclization*; Emmett, P. H., Ed.; Reinhold: New York, 1956; Vol. IV, pp 237–242. (b) Pichler, H.; Buffleb, H. *Brennst.-Chem.* **1940**, *21*, 257, 273, 285.

(6) George, P. M.; Avery, N. R.; Weinberg, W. H.; Tebbe, F. N. *J. Am. Chem. Soc.* **1983**, *105*, 1393–1394.

(7) Carter, E. A.; Goddard, W. A., III *J. Am. Chem. Soc.* **1986**, *108*, 2180.

(8) (a) van Asselt, A.; Burger, B. J.; Gibson, V. C.; Bercaw, J. E. *J. Am. Chem. Soc.* **1986**, *108*, 5347. (b) Parkin, G.; Bunel, E.; Burger, B. J.; Trimmer, M. S.; van Asselt, A.; Bercaw, J. E. *J. Mol. Catal.*, in press.

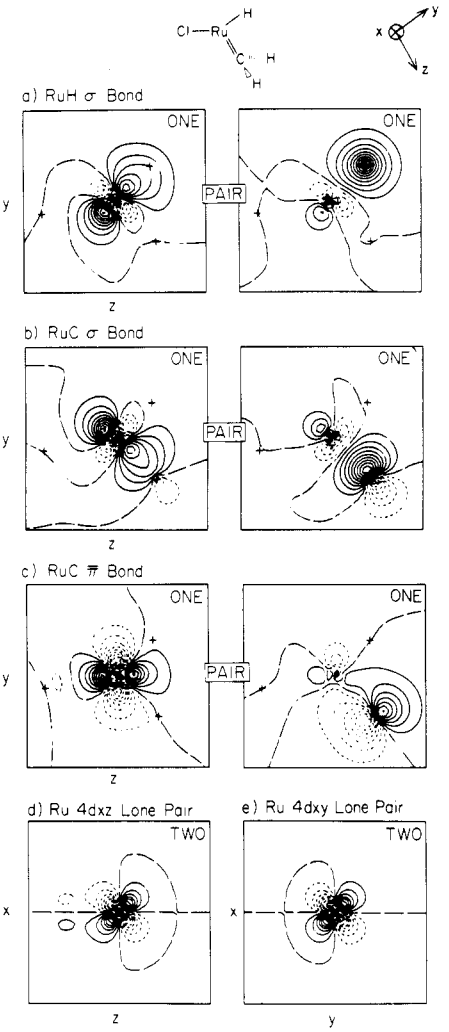

Figure 1. GVB(3/6)PP one-electron orbitals for **1a**, the σ^3 state of $ClRu(CH_2)H$ at its optimum geometry: (a) the Ru–H bond; (b) the Ru–C σ bond; (c) the Ru–C $\bar{\pi}$ bond; (d) the Ru doubly occupied $4d_{xz}$ orbital; and (e) the Ru doubly occupied $4d_{xy}$ orbital. Long dashes indicate zero amplitude, and the spacing between contours is 0.05 au.

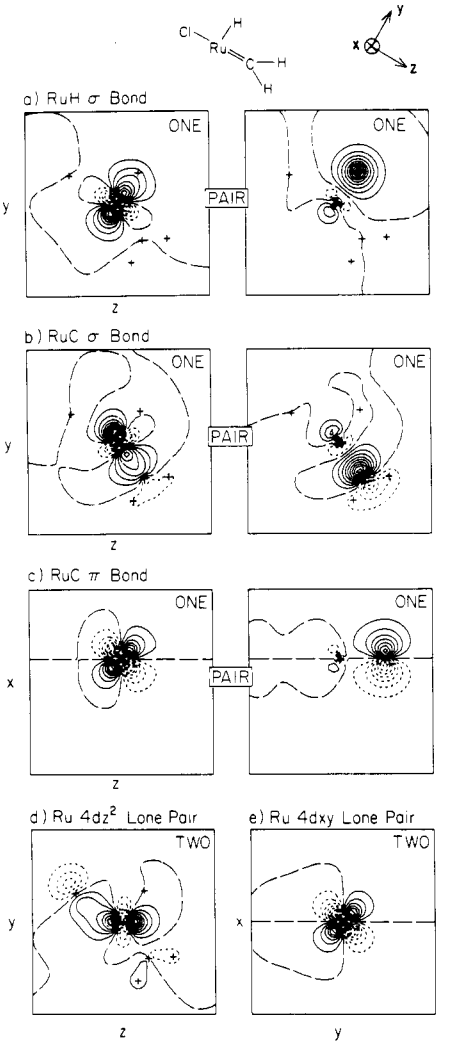

Figure 2. GVB(3/6)PP one-electron orbitals for **1b**, the $\sigma^2\pi$ state of $ClRu(CH_2)H$ at its optimum geometry: (a) the Ru–H bond; (b) the Ru–C σ bond; (c) the Ru–C π bonds; (d) the Ru doubly occupied $4d_{z^2}$ orbital; and (e) the Ru doubly occupied $4d_{xy}$ orbital.

a total of nine orbitals or 18 electrons for $Cp^*_2Ta(H)(CH_2)$ and eight orbitals or 16 electrons for $Cp^*_2Ta–CH_3$. Thus **4** is analogous to **1** and **5** is analogous to **2**.

To date, no direct measurements of thermodynamic properties for the migratory insertion of CH_2 into M–H have been published and only one case has been reported involving kinetic data for such an insertion (for Ta).[8b] Our goal was to examine the nature of this reaction at a single metal center, characterizing the qualitative features of the metal–ligand bonding which favor (or disfavor) migratory insertions of CH_2, and to predict the quantitative aspects of the insertion potential energy surface (e.g., the activation barrier and the exothermicity).

In the next section, we discuss the equilibrium properties of the hydrido methylidene **1**. Section III presents detailed theoretical results on the migratory insertion itself,[9] while section IV discusses an independent way of estimating the energetics of the insertion event. Using correlation-consistent configuration interaction (CCCI),[10] we obtain the exothermicity and activation barrier to insertion as a function of both basis set and level of electron correlation via a thermodynamic cycle that utilizes metal–ligand bond energies obtained from CCCI calculations. Section V concludes with some speculations regarding other insertion steps in FT chemistry, while section VI provides the calculational details.

II. Properties of $ClRu(CH_2)H$

To understand the electronic structure of the $^1A'$ state of **1**, we consider how the ClRu fragment may bond to H and CH_2. Starting with the ground state of Ru, s^1d^7, the Cl ligand of $ClRu(CH_2)H$ ties up the Ru s electron in an ionic bond, leaving a high spin d^7 electronic configuration (2 2 1 1 1) on Ru. Classifying the five d orbitals with respect to the final molecular plane as σ or π, there are two important configurations of ClRu: $(d\sigma_1)^1(d\sigma_2)^1(d\sigma_3)^1(d\pi_1)^2(d\pi_2)^2$, which we denote as σ^3, and $(d\sigma_1)^1(d\sigma_2)^1(d\sigma_3)^2(d\pi_1)^1(d\pi_2)^2$, which we denote as $\sigma^2\pi$. Bonding the σ^3 configuration to CH_2 and H leads to[11] a twisted structure **1a** with all three M–H and M–C bonds in the H–Ru–C plane, while bonding the $\sigma^2\pi$ configuration to CH_2 and H

(9) A preliminary account of the insertion results has already appeared: Carter, E. A.; Goddard, W. A., III *J. Am. Chem. Soc.* **1987**, *109*, 579.

(10) (a) Carter, E. A.; Goddard, W. A., III *J. Chem. Phys.*, in press. (b) *J. Chem. Phys.*, in press.

(11) The lowest energy structure of **1a** retains C_s symmetry (i.e., lower symmetry structures for both **1a** and **1b** were found to be higher in energy), but the CH_2 ligand is bent 4.1° out of the idealized $RuCH_2$ plane, toward the Cl ligand. However, the cost to make Ru and the CH_2 ligand coplanar is only 0.08 kcal/mol, and hence we discuss the $RuCH_2$ unit as if it were coplanar.

Table I. Orbital Overlaps, Metal Orbital Hybridization, and Bond Populations[a] for the GVB Bond Pairs in 1a and 1b

complex	bond	overlap	Ru hybridization % 5sp	Ru hybridization % 4d	bond pop.[b] Ru	bond pop.[b] X
1a (σ^3)	Ru–C σ	0.73	18.8	81.2	0.96	1.03
1a (σ^3)	Ru–C π	0.50	4.4	95.6	1.10	0.88
1a (σ^3)	Ru–H	0.69	25.6	74.4	1.02	0.95
1a (σ^3)	Ru–Cl	0.90	64.7	35.3	0.38	1.62
1b ($\sigma^2\pi$)	Ru–C σ	0.71	17.8	82.2	0.93	1.03
1b ($\sigma^2\pi$)	Ru–C π	0.41	2.2	97.8	1.07	0.93
1b ($\sigma^2\pi$)	Ru–H	0.63	15.6	84.4	1.08	0.91
1b ($\sigma^2\pi$)	Ru–Cl	0.88	84.5	15.5	0.35	1.64

[a] Reference 13. [b] A perfectly covalent bond has a bond population of 1.00 for Ru and 1.00 for X (X = CH_2, H, or Cl).

results in a planar structure **1b** which has an out-of-plane π bond.[12]

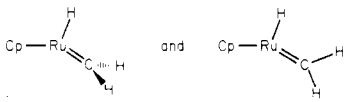

1a **1b**

The generalized valence bond (GVB) orbitals (each containing *one* electron) for both conformers are shown in Figures 1 and 2. Here we see that the Ru–H and Ru–C bonds are quite covalent, with each bond pair involving a spin pair between one electron localized in an Ru d orbital and one electron localized on a ligand. In both cases, the CH_2 fragment is best viewed as a *neutral* triplet CH_2 with one electron in each of the σ and π nonbonding orbitals

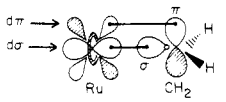

spin-paired with singly occupied dσ and dπ orbitals on Ru, forming an Ru=C covalent double bond as in ethylene.[7] For the σ^3 state of RuCl, the π bond involves an in-plane dπ orbital; we denote this as d$\bar{\pi}$ to distinguish this from the out-of-plane dπ orbital.

The GVB orbital properties are listed in Table I. For the bonds to C and H, the 4d character of the metal bonding orbitals ranges from 74 to 98%, with less than 11% ionic character in each bond pair.[13] For the Ru–Cl bonds, approximately 0.6 electron is transferred from Ru to Cl in both **1a** (0.62 electron) and **1b** (0.64 electron), so that one should visualize the Ru–Cl bond as mostly ionic but partially covalent, involving 65–85% 5s–5p hybrid character on Ru.

Table II. Optimized Structural Parameters and Harmonic Vibrational Frequencies for 1a and 1b[a]

parameter	complex **1a** (σ^3)	complex **1b** ($\sigma^2\pi$)
R_e(Ru–C) (Å)	1.90	1.92
R_e(Ru–H) (Å)	1.65	1.63
R_e(Ru–Cl) (Å)	2.42	2.43
θ_e(H–Ru–C) (deg)	90.3	111.7
θ_e(H–Ru–Cl) (deg)	145.1	93.6
θ_e(H–C–H) (deg)	120.0	121.1
ω_e(Ru=C) (cm^{-1})	747 (0.9262)[b]	798 (1.060)[b]
ω_e(Ru–H) (cm^{-1})	2021 (0.5464)[b]	1825 (0.4492)[b]
ω_e(Ru–Cl) (cm^{-1})	420 (0.6259)[b]	353 (0.4414)[b]
ω_e(HCH scissors) (cm^{-1})	1487 (4.737 × 10^{-5})[c]	1416 (4.291 × 10^{-5})[c]

[a] Optimized at the GVB-RCI(3/6) level (section VI). [b] Force constant in hartree/Å^2. [c] Force constant in hartree/deg^2.

Denoting the Ru=C and Ru—H axes as z and y, the Ru—C $\bar{\pi}$ bond (π bond in the plane) in **1a** involves the $4d_{yz}$ orbital, while the Ru—C σ and Ru—H bonds involve orbitals that are mainly $4d_{z^2}$ and $4d_{y^2}$. Since the $\bar{\pi}$ bond involves the $4d_{yz}$ orbital, we expect (and find) a 90° H–Ru–C bond angle so that the Ru–H and Ru–C σ-bond orbitals will be orthogonal to the Ru–C $\bar{\pi}$ bond. The optimum structural parameters[14] for geometry **1a** are listed in Table II and depicted below:

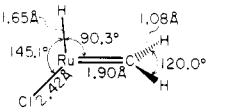

As mentioned in the Introduction, d^3 Ta(II) should form bonds similar to d^7 Ru(I), since both metals have three unpaired d electrons to form covalent bonds to H(R) and CH_2. Thus, the Ru—H and Ru=CH_2 bonds in **1a** should be quite analogous to the Ta—CH_3 and Ta=CH_2 bonds in Schrock's complex $Cp_2Ta(CH_3)(CH_2)$ (**4**).[15] In fact, the Ru=C bond length, the H—Ru—C bond angle, and the perpendicular orientation of the CH_2 ligand all compare well with the values R(Ta=C) = 2.03 Å, θ(CTaC) = 95.6°, and the out-of-plane orientation of the CH_2 ligand found in **4**.[15] Another complex electronically similar to **1** is Cl(NO)$(PPh_3)_2$Os(CH_2) (**5**), in which the NO and PPh_3 ligands are simulated by the H ligand and the low-spin state in **1**. The X-ray structure of **5** reveals an Os=C bond length of 1.92 Å and an orientation for the CH_2 ligand which is perpendicular to the N—Os—C plane,[16] in

(12) Complexes **1a** and **1b** are taken to be singlet spin states as models for coordinatively saturated organometallic complexes. Similar low-spin models with only a few ligands have recently been used in ab initio studies of CO insertion (Dedieu, A.; Sakaki, S.; Strich, A.; Siegbahn, P. E. M. *Chem. Phys. Lett.* **1987**, *133*, 317). Since ^{1}A′ spin states are used for **1**, we consider only the triplet spin states of ClRuH (obtained when the bond of Ru=C bond is broken). However, the actual ground state of ClRuH(CH_2) is a ^{3}A″ state wherein all three bonds to H and CH_2 are maintained. The singlet "σ^3" state we have chosen to examine lies (at least) 16.8 kcal/mol higher in energy at the GVBCI(4/8) level of theory [which consists of a full CI among the six orbitals of the three bond pairs and the two high-spin orbitals for ClRu(CH_2)H (^{3}A″) and of a full CI among the eight orbitals corresponding to the three bond pairs plus the singlet Ru 4d lone pair for ClRu(CH_2)H (^{1}A′)]. We did not optimize the structure of the ^{3}A″ state of ClRu(CH_2)H, so that 16.8 kcal/mol is a lower bound on the ^{1}A′ – ^{3}A″ energy difference. The ^{3}A″ ground state of ClRu(CH_2)H may be understood as follows. In the ^{1}A′ state, the σ and π bonds to H and CH_2 (choosing the H–Ru–C plane as yz) utilize $4d_{yz}$, $4d_{z^2}$, $4d_{y^2}$, and 5s character on the metal, while $4d_{x^2}$ character is not used at all. In the triplet state, the $4d_{x^2}$ and $4d_{xz}$ orbitals are singly occupied, gaining favorable exchange terms between the high-spin electrons *without losing any of the metal–ligand bonding*, leading to a triplet ground state. Correspondingly, the ground state of ClRuH is actually a linear $^5\Delta$ state, derived from the (excited state) s^2d^6 valence electron configuration on Ru.

(13) The electron populations were calculated by summing over Mulliken populations for the first and second natural orbitals of each GVB pair.

(14) All angles and bond lengths were optimized at the GVB-RCI(3/6) level (section VI) in complexes **1a** and **1b**, except for R(C–H), which was fixed at 1.08 Å.

(15) Guggenberger, L. J.; Schrock, R. R. *J. Am. Chem. Soc.* **1975**, *97*, 6578.

(16) Hill, A. F.; Roper, W. R.; Waters, J. M.; Wright, A. H. *J. Am. Chem. Soc.* **1983**, *105*, 5939.

agreement with our results for **1**.

The Ru=CH_2 stretching frequencies are calculated to range from 740 to 800 cm^{-1} (Table II), which may be compared with 623.6 cm^{-1} for matrix-isolated $FeCH_2$.[17] (No other M=CH_2 vibrational frequencies have been identified.) The Ru=C stretching frequency of **1b** is larger than in **1a** by ~50 cm^{-1}. This may be understood in terms of the larger steric repulsions in **1b** relative to **1a**, since the methylidene hydrogens are coplanar with the rest of the molecule in **1b**, whereas they are out of the plane in **1a**. Such steric repulsions induce a harder inner wall of the local potential, leading to an increased Ru=C vibrational frequency. The decrease in the Ru–H vibrational frequency going from **1a** to **1b** may be attributed to the decrease in the overlap in the Ru–H bond (Table I), indicating a shallower potential and thus a lower vibrational frequency in **1b**.

The calculated rotational barrier of 13.6 kcal/mol for **1a** → **1b** is smaller than the lower bound of 21.4 kcal/mol estimated for **4**.[15] This is to be expected, since the Cp ligands in the Ta complex should destabilize the π orbitals required to make the out-of-plane π bond in **4**, thereby increasing the rotational barrier. In a related system, Brookhart[18] has measured the rotational barrier in Cp-($Ph_2PCH_2CH_2PPh_2$)$FeCH_2^+$ (Ph = C_6H_5) to be 10.4 kcal/mol, in reasonable agreement with our results.

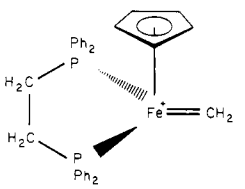

The structural coordinates and vibrational frequencies for geometry **1b** (see Table II) are similar except that the H–Ru–C angle opens up to 111.7° and the H–Ru–Cl angle drops to 93.6°.

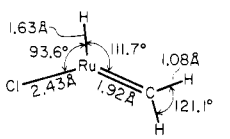

In this case, there is a doubly occupied dσ orbital bisecting the H–Ru–C bond angle (see Figure 2), and the Ru–H and Ru–C dσ orbitals must stay orthogonal to this orbital, forcing a larger H–Ru–C bond angle. The Cl ligand must also stay orthogonal to the in-plane dσ orbital and thus moves away, resulting in a smaller Cl–Ru–H angle.

As the Ru–C bond distance is increased to break the Ru=CH_2 bond, **1a** correlates with the ClRuH complex **6a** in the $(\sigma_1)^1(\sigma_2)^1$ triplet state $^3A'$ (σ^3 configuration of ClRu), while **1b** correlates with **6b** in the $(\sigma_1)^1(\pi)^1$ triplet state $^3A''$ ($\sigma^2\pi$ configuration of ClRu). These states of ClRuH are

6a **6b**

separated by over 4.2 kcal/mol, with $^3A''$ lower.[19] Thus, even though the lowest triplet state of ClRuH is $\sigma^2\pi$,[11] the favored geometry of ClRuH(CH_2) ($^1A'$) corresponds to the σ^3 state. This means that the stabilization enjoyed by the σ^3 state of **1a** over the $\sigma^2\pi$ state of **1b** is determined by the Ru–C bonds rather than by the intrinsic energies of the ClRuH fragment. That is, the *in-plane $\bar{\pi}$ bond* of **1a** versus the out-of-plane π bond of **1b** contributes to the stabilization of **1a** over **1b**. Consistent with this idea, Table I indicates that the most dramatic increase in orbital overlaps occurs for the out-of-plane π bond (**1b**) converting to an in-plane $\bar{\pi}$ bond (**1a**). Another factor that destabilizes **1b** relative to **1a** is the higher steric (or nuclear) repulsion in **1b**, since all of the atoms are coplanar.

III. Migratory Insertion Kinetics

For the methylidene insertion step (1) relevant to Fischer–Tropsch catalysis, we find the structure **1a**, with the *in-plane π bond*, to be the relevant conformation. Consider the transformation of the Ru—H bond and the Ru=C double bond (prior to insertion) to a C—H bond, an Ru—C single bond, and an Ru 4d lone pair. We find a sequence (eq 10) involving the rearrangement of the three in-plane bonding pairs,[20] where the orbitals of the Ru–C

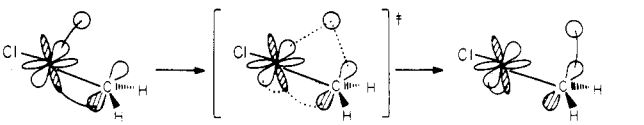

(10)

$\bar{\pi}$ bond mix with the orbitals of the Ru–H σ bond in order to make the new C–H σ bond and an Ru 4d lone pair. Structure **1a** (σ^3) has a carbon p orbital in the H–Ru–C plane (part of the $\bar{\pi}$ bond) that is oriented such that a smooth conversion from Ru–H to C–H is possible, whereas structure **1b** ($\sigma^2\pi$) has a π bond perpendicular to the H–Ru–C plane such that the carbon p orbital needed for the incipient C–H bond is orthogonal to the insertion pathway. This suggests that *only systems containing alkylidenes oriented perpendicular to adjacent bonds* (with an in-plane π bond as in **1a**) will have low barriers to migratory insertion.

A. The Barrier. We find indeed that the insertion reaction (7) (involving **1a** with its in-plane π bond) is favorable, proceeding with a low barrier of 11.5 kcal/mol and an exothermicity of 7.1 kcal/mol.[9] Figure 3 displays the reaction path energetics for five levels of theory. Analytic gradients of Hartree–Fock (HF, variational molecular orbital theory) wave functions were used to optimize the geometries at the nine points shown along the insertion pathway. The H–Ru–C angle was taken to be the reaction coordinate, with each successive H–Ru–C angle held fixed while all other geometrical parameters were optimized (within C_s symmetry). The geometries of **1a** and **2** were optimized by using HF gradients with no constraints except the retention of C_s symmetry.[11,21]

(17) Chang, S.-C.; Kafafi, Z. H.; Hauge, R. H.; Billups, W. E.; Margrave, J. L. *J. Am. Chem. Soc.* **1985**, *107*, 1447.

(18) Brookhart, M.; Tucker, J. R.; Flood, T. C.; Jensen, J. *J. Am. Chem. Soc.* **1980**, *102*, 1203.

(19) The optimum geometry [at the GVB(1/2)-PP level] of $^3A'$ has θ(Cl–Ru–H) = 104.8°, R(Ru–H) = 1.64 Å, and R(Ru–Cl) = 2.38 Å. The $^3A'$ – $^3A''$ energy splitting of 4.2 kcal/mol is a lower bound since the geometry of the $^3A''$ state was kept fixed at the optimum geometry for the $^3A'$ state (only the equilibrium geometry of the $^3A'$ state was needed in later calculations).

(20) For spin-conserved processes, the resultant insertion product is $^1A'$ $ClRuCH_3$, *not* $^3A'$ $ClRuCH_3$.

(21) HF wave functions are reliable for predicting accurate geometries. The HF and the RCI(3/6) optimum geometries of **1a** are very similar, with the Ru–Cl, Ru–H, and C–H bond lengths identical for both levels of theory. The other HF geometrical parameters for **1a** are R(Ru=C) = 1.87 Å, θ(H–Ru–C) = 82.7°, θ(H–Ru–Cl) = 157.0°, and θ(H–C–H) = 113.3°. These values differ from the RCI(3/6) optimum geometry by no more than 0.03 Å and 11.9° (where the latter difference is large due to the flat potential felt by the Cl ligand). The HF energies for these two geometries are –4936.363 10 and –4936.359 58 hartrees for the HF gradient and the RCI(3/6) optimizations, respectively. These small changes in energy (2.2 kcal/mol) and structure between the two geometries support the use of HF gradient-optimized geometries in this study.

Table III. Energetics (kcal/mol) for the CH_2 Insertion into the Ru–H Bond in $ClRuH(CH_2)$ within a VDZ Basis[a]

calculation	spatial config/ SEF[c]	total energies (hartrees)[b] 1a	TS[d]	2	ΔE_{rxn}	E_a[e]	θ(H–Ru–C),[†e]
HF	(1/1)	−4936.363 11	−4936.363 11	−4936.425 11	−38.9	0.0	82.7
GVB(3/6)-PP	(8/8)	−4936.439 66	−4936.424 43	−4936.474 22	−21.7	9.7	51.2
GVB-RCI(3/6)	(27/37)	−4936.463 72	−4936.437 08	−4936.480 20	−10.3	16.7	47.7
GVBCI(3/6)	(141/175)	−4936.469 40	−4936.448 21	−4936.481 74	−7.7	13.4	45.2
GVBCI(3/6)-MCSCF	(141/175)	−4936.471 18	−4936.453 01	−4936.482 42	−7.1	11.5	48.8

[a] Calculational details are provided in sections III and VI. [b] 1 hartree = 627.5096 kcal/mol. [c] The number of spatial configurations/spin eigenfunctions associated with each calculation. [d] TS = transition state. The total energies listed under TS are values for points calculated nearest the true TS and its associated θ(H–Ru–C)† (i.e., HF energy is for $\theta^\dagger$ = 82.7°, GVB-PP for 50.0°, RCI for 47.5°, GVBCI for 45.0°, and GVBCI-MCSCF for 50.0°). [e] The proper method of calculating the activation barrier is by fitting the data points to a potential maximum; the values listed for E_a and θ(H–Ru–C)† are obtained in this manner. Using the differences in total energies for the nearest points to the TS leads to a decrease in E_a by 0.1 kcal/mol for the GVB-PP and the two GVBCI calculations.

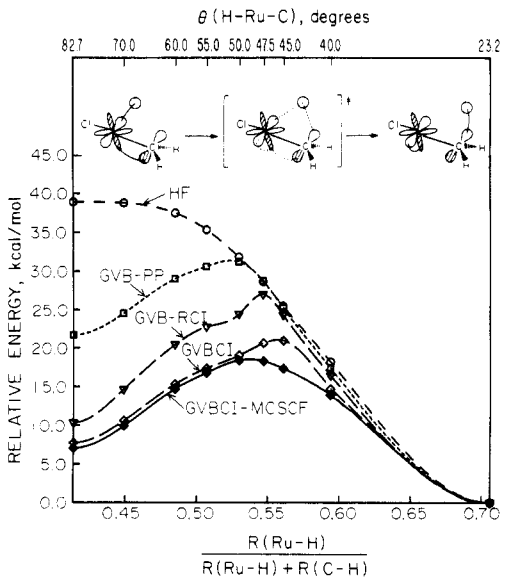

Figure 3. Reaction coordinate for the insertion of CH_2 into Ru–H in **1a** to form **2** at the HF, GVB(3/6)-PP, GVB-RCI(3/6), GVBCI(3/6), and GVBCI(3/6)-MCSCF levels of theory. Energy (kcal/mol) is plotted relative to the total energy of **2** vs the normalized reaction coordinate R(Ru–H)/[R(Ru–H) + R(C–H)]. The corresponding H–Ru–C angles (deg) are indicated at the top. The full GVBCI-MCSCF wave function yields simultaneously a proper description of reactant, transition state, and product, resulting in a smooth potential curve. Some lower level wave functions lead to less smooth transitions, since they are less capable of describing both reactant and product channels.

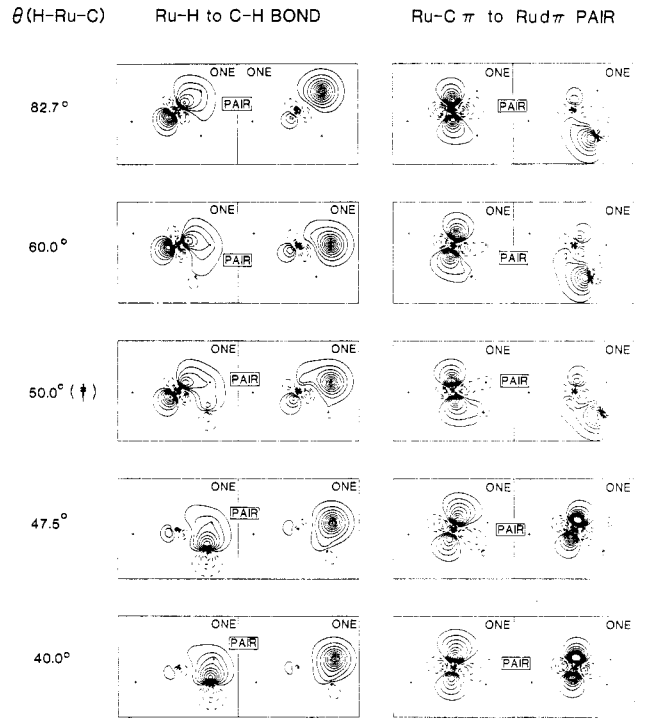

Figure 4. GVB(3/6)PP one-electron orbitals along the reaction path for the Ru–H bond of **1a** converting to the C–H bond of **2** and for the Ru–C $\bar{\pi}$ bond of **1a** converting to the Ru dπ pair of **2**. Reaction coordinate shown as θ(H–Ru–C), where the reactant has θ(H–Ru–C) = 82.7°, the transition state at 50.0°, and the product at 23.2°. (Nodal lines have been omitted for clarity.)

Table III, in conjunction with Figure 3, displays the trends in exothermicity and activation energy as a function of increasing electron correlation. Notice that Hartree–Fock theory, while generally reliable for structural predictions,[21] leads to reaction energetics in serious disagreement with the highest quality wave function, GVBCI-MCSCF (see section VI). HF predicts a highly exothermic reaction (ΔE_{rxn} = −38.9 kcal/mol) with no barrier, while GVBCI-MCSCF predicts a much more moderate exothermicity of 7.1 kcal/mol and a moderate barrier of 11.5 kcal/mol. The reason HF describes the reaction energetics so poorly is the inability of HF theory to properly describe transition metal–ligand π bonds. The HF restriction that each orbital be doubly occupied causes the π bond to localize on the metal (to get unit overlap) and the σ bond to localize on the carbon, leading to singlet carbene and a very weak double bond.[22] With the metal–carbene bond in **1a** ill-described, the reactant is highly destabilized, leading to an artificially large exothermicity. Because of this fundamental problem, recent HF-Slater calculations of large exothermicities for migratory insertion of CH_2 into an Mn–H bond are probably incorrect.[23] Similarly, recent HF predictions of the energetics of CO insertion at Mn likely have large (>20 kcal/mol) errors.[24]

In the GVB wave functions, each of the six electrons involved in the insertion reaction (two in the Ru—H bond and four in the Ru=C bond) are allowed the freedom to occupy their own orbitals. This results in a good description of metal–ligand multiple bonds.[7,22,25a] Thus, the simplest inclusion of electron correlation (GVB-PP) where each MO pair is described with two orbitals gives rise to a large stabilization of the reactant relative to HF, with

(22) Carter, E. A.; Goddard, W. A., III *J. Phys. Chem.* **1984**, *88*, 1485.

(23) Ziegler, T.; Versluis, L.; Tschinke, V. *J. Am. Chem. Soc.* **1986**, *108*, 612.

(24) Axe, F. U.; Marynick, D. S. *Organometallics* **1987**, *6*, 572.

(25) (a) Carter, E. A.; Goddard, W. A., III *J. Phys. Chem.*, in press. (b) While the exothermicity and barrier may change slightly due to the presence of additional ancillary ligands, the dominant contribution to the energetics is dictated by electronic effects, as indicated by the strong dependence of the energetics on electron correlation. Since the electronic effects are included in our model, we believe the exothermicity and barrier to be representative of insertion kinetics for late-transition-metal methylidenes.

Table IV. Changes in the Hartree-Fock Geometry along the Reaction Coordinate

θ(H–Ru–C) (deg)	82.7[a]	70.0	60.0	55.0	50.0	47.5	45.0	40.0	23.2[b]
R_e(Ru–H) (Å)	1.65	1.68	1.72	1.75	1.77	1.83	1.85	1.94	2.63
R_e(C–H) (Å)	2.33	2.05	1.82	1.70	1.57	1.51	1.45	1.33	1.10
R_e(Ru–C) (Å)	1.87	1.89	1.91	1.92	1.93	1.93	1.93	1.94	2.06
R_e(Ru–Cl) (Å)	2.42	2.41	2.40	2.40	2.38	2.39	2.38	2.37	2.36
R_e(C–H')[c] (Å)	1.09	1.08	1.08	1.08	1.09	1.08	1.08	1.08	1.09
θ_e(H'CH') (deg)	113.3	112.4	112.2	112.2	110.9	112.4	112.5	112.5	108.6
θ_e(Cl–Ru–C) (deg)	120.3	130.2	134.3	138.9	142.0	135.4	135.5	132.1	105.4
θ_e(H'–C–Ru) (deg)	123.4	123.7	123.7	123.8	124.4	123.8	123.6	122.9	110.5

[a] The optimum angle for **1a** at the HF level. [b] The optimum angle for **2** at the HF level. [c] Unprimed hydrogen is the migrating hydrogen.

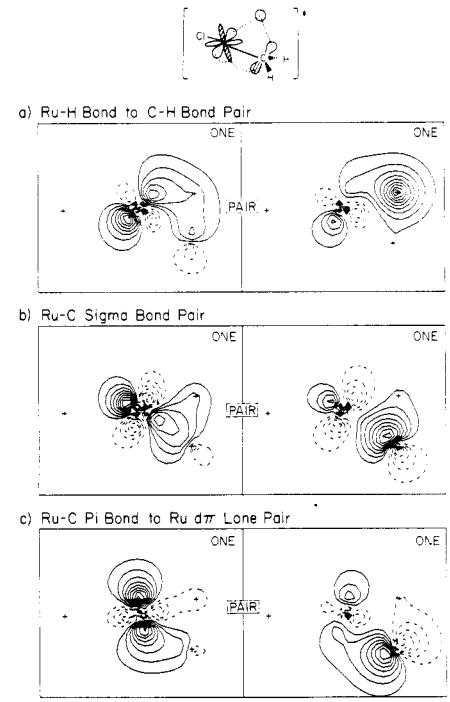

Figure 5. GVB(3/6)PP one-electron orbitals near the transition state [θ(H–Ru–C)‡ = 50.0°]: (a) orbital pair describing the Ru–H bond of reactant **1a** and the C–H bond of product **2**; (b) the Ru–C σ bond; (c) orbital pair describing the Ru–C $\bar{\pi}$ bond of **1a** and the Ru 4d lone pair of **2**.

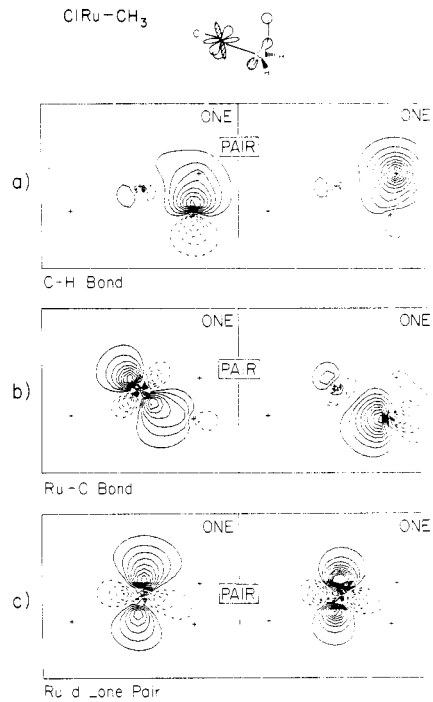

Figure 6. GVB(3/6)PP one-electron orbitals in the product channel [θ(H–Ru–C)‡ = 40.0°]: (a) the C–H bond of product **2**; (b) the Ru–C σ bond; (c) the Ru 4d lone pair of **2**.

a decrease in the exothermicity by 17.2 kcal/mol and the appearance of a barrier (9.7 kcal/mol). Allowing full freedom for these six electrons within the six active orbitals involved in the insertion (a full valence GVBCI, i.e., all occupations of the six electrons in the six orbitals) includes resonance effects that reduce the activation barrier. Optimizing the orbitals self-consistently at the GVBCI level includes resonance more completely, resulting in a barrier of 11.5 and an exothermicity of –7.1 kcal/mol.[25b] This may be compared with a recent experimental determination of the activation barrier ($\Delta G^\ddagger$) of 16.2 ± 0.5 kcal/mol at 50 °C for the migration of H to CH_2 in $(C_5Me_5)_2Ta(H)(=CH_2)$.[8b] The activation barrier is expected to be higher for Ta than for Ru, since the insertion is thought to be endothermic for Ta (much stronger M=C π bonds).

B. Orbital Correlations. Figure 4 shows the evolution of the four active orbitals comprising the Ru–H (and incipient C–H) bond and the Ru–C π bond (and incipient Ru dπ pair) from the reactant **1a** [θ(H–Ru–C) = 82.7°], through the transition state [θ(H–Ru–C) = 50.0°], and into the product channel [θ(H–Ru–C) = 40.0°]. The Ru–C σ bond is not shown here, since it does not change significantly during the insertion (see Figures 1, 5, and 6). These two bond pairs change smoothly from reactants to products, converting the Ru–H bond of **1a** into the C–H bond of **2** and the Ru–C $\bar{\pi}$ bond of **1a** into the Ru 4d lone pair of **2**. At the transition state, the Ru–C $\bar{\pi}$ bond (Figures 4 and 5) is beginning to move out of the way of the incipient C–H bond, with some 4d lone pair character evident. The barrier to reaction is kept moderate by the ability of the active orbitals to maintain high overlap in the transition region so that no bonds are weakened significantly.[26] Finally, we note that the orbitals in Figure 6 [θ(H–Ru–C) = 40.0°] are presented as product orbitals, merely to emphasize that once past the transition region, the orbitals quickly adopt the characteristics of product, even just 10° past the transition state geometry. (The H–Ru–C "bond angle" in the product **2** is 23.2°.)

The changes in the geometry as the insertion proceeds are shown in Table IV. The Ru–H bond length smoothly increases from 1.65 in **1a** to 2.63 Å in **2**, while the incipient C–H bond decreases smoothly in length from the nonbonded distance of 2.33 Å in **1a** to the equilibrium distance of 1.10 Å in **2**. The Ru=C double bond length of 1.87 Å in **1a** also smoothly increases to the Ru—C single bond length of 2.06 Å. Other geometrical parameters change also, but with less marked differences.

In the next section, we discuss higher level calculations aimed at determining the effect of extended basis sets and of higher electron correlation on the barrier and exothermicity of the insertion process.

IV. Insertion Thermochemistry

We performed additional calculations in order to provide an independent assessment of the activation barrier and

(26) (a) Steigerwald, M. L.; Goddard, W. A., III *J. Am. Chem. Soc.* **1984**, *106*, 308. (b) *Ibid.*, submitted for publication.

Table V. Adiabatic Ru=CH_2 Bond Energies (D_e) in ^{1}A′ ClHRu=CH_2 (kcal/mol)[a]

calculation	basis set[b]	total energies (hartrees)[c] ^{1}A′ ClRuH(CH_2)	^{3}A′ ClRuH	$^3B_1$ CH_2	D_e(Ru=C)
HF	VDZ	−4936.359 58 (1/1)	−4897.424 64 (1/1)	−38.913 49 (1/1)	13.5
GVB-PP	VDZ	−4936.441 92 (8/8)	−4897.455 42 (2/2)	−38.913 49 (1/1)	45.8
GVB-RCI	VDZ	−4936.466 69 (27/37)	−4897.457 36 (3/5)	−38.913 49 (1/1)	60.1
RCI*s_{val}	VDZ	−4936.512 58 (1899/3997)	−4897.468 50 (117/295)	−38.920 67 (14/28)	77.4
CCCI[d]	VDZ	−4936.516 76 (4979/9725)	−4897.468 50 (117/295)	−38.920 67 (14/28)	80.1
GVB-PP	VDZD	−4936.454 22 (8/8)	−4897.455 42 (2/2)	−38.923 31 (1/1)	47.4
GVB-RCI	VDZD	−4936.477 49 (27/37)	−4897.457 36 (3/5)	−38.923 31 (1/1)	60.8
RCI*[$SD_{Ru-C\sigma}$ + $SD_{Ru-C\pi}$]	VDZD	−4936.500 89 (5465/9619)	−4897.461 42 (67/109)	−38.923 31 (1/1)	72.9
CCCI	VDZD	−4936.538 49 (7127/13895)	−4897.468 50 (117/295)	−38.935 03 (22/44)	84.7

[a] Details of the calculations are provided in section VI. [b] VDZ: valence double-ζ bases were used for all atoms except Cl [treated by using an SHC-EP for the core electrons and an MBS (minimum basis set) description of the valence electrons. VDZD: same basis set as VDZ except one set of d-polarization functions was added to the C basis (ζ = 0.64). See Section VI. [c] 1 hartree = 627.5096 kcal/mol. The number of spatial configurations/spin eigenfunctions associated with each calculation is given in parentheses under each total energy. [d] CCCI ≡ RCI*[$SD_{Ru-C\sigma}$ + $SD_{Ru-C\pi}$ + S_{val}].

Table VI. Adiabatic Singlet-Triplet Splittings (ΔE_{ST}) in ClRuH (kcal/mol)[a]

calculation[b]	basis set[c]	total energies (hartrees) ^{1}A′	^{3}A′	ΔE_{ST}
GVB-PP	VDZP	−4897.428 51 (4/4)	−4897.456 50 (2/2)	17.6
RCI	VDZP	−4897.428 55 (9/10)	−4897.458 41 (3/5)	18.7
RCI*$SD_{Ru\,d\sigma's}$	VDZP	−4897.438 29 (389/490)	−4897.464 36 (348/550)	16.4
CCCI[d]	VDZP	−4897.445 04 (555/760)	−4897.472 04 (408/778)	16.9
CCCI	VDZ	−4897.443 20 (425/581)	−4897.470 13 (304/584)	16.9

[a] $\Delta E_{ST} = E_{singlet} - E_{triplet}$. [b] Calculational details provided in section VI. [c] VDZP: VDZ Ru, SHC-EP + MBS Cl, and DZP H. VDZ: same as VDZP but the unscaled p function on H was removed (section VI). [d] CCCI ≡ RCI*[$SD_{Ru\,d\sigma's}$ + S_{val}].

exothermicity for the insertion reaction. In addition to the five levels of theory used above to map out the potential energy surface of the insertion shown in (7), we carried out studies using larger basis sets along with the inclusion of higher order correlations in the configuration interaction (CI) calculation.

Calculating the bond energies for the metal–ligand bonds in **1a** and **2**, we can construct a thermodynamic cycle to predict the exothermicity of (7), as shown in Figure 7. The energetics for each step in the cycle were calculated by using the CCCI method[10] (see section VI) within both a valence double-ζ (VDZ) basis and polarized VDZ bases (VDZD, VDZP, and VDZDP). The CCCI method has proved to yield accurate predictions of energetics, resulting in bond dissociation energies and excitation energies for both organic and organometallic molecules within 5 kcal/mol of the experimental values.[10,25,27]

We calculated the steps leading to ClRu (^{2}A′) + H (^{2}S) + CH_2 ($^3B_1$) at the top of Figure 7, starting from the reactant **1a** at the bottom left or from the product **2** at the bottom right and following the cycle upward, in order to obtain the relative energies of **1a** and **2**. Tables V–IX display results for D_e(Ru=C), ΔE_{ST} (ClRuH), D_e(Ru—H), D_e(Ru—C), and D_e(H_2C—H), as a function of basis set and

(27) Hanratty, M. A.; Carter, E. A.; Beauchamp, J. L., Goddard, W. A., III *Chem. Phys. Lett.* **1986**, *123*, 239.

Table VII. Adiabatic Ru-H Bond Energies (D_e) in ^{1}A′ ClRuH (kcal/mol)[a]

calculation	basis set[b]	total energies (hartrees)[c] ^{1}A′ ClRuH	^{2}A′ ClRu	D_e(Ru-H)
HF	VDZ	−4897.393 40 (1/1)	−4896.857 40 (1/1)	23.0
GVB-PP	VDZ	−4897.427 33 (4/4)	−4896.861 88 (2/2)	41.5
RCI	VDZ	−4897.427 37 (9/10)	−4896.861 88 (3/4)	41.5
RCI*SD_{Ru-H}	VDZ	−4897.430 14 (289/361)	−4896.861 97 (32/42)	43.2
CCCI[d]	VDZ	−4897.441 47 (425/581)	−4896.862 58 (76/152)	50.0
HF	VDZP	−4897.395 05 (1/1)	−4896.857 40 (1/1)	24.1
GVB-PP	VDZP	−4897.428 51 (4/4)	−4896,861 88 (2/2)	42.3
RCI	VDZP	−4897.428 55 (9/10)	−4896.861 88 (3/4)	42.3
RCI*SD_{Ru-H}	VDZP	−4897.436 16 (389/490)	−4896.861 97 (32/42)	47.0
CCCI	VDZP	−4897.448 12 (555/760)	−4896.862 58 (76/152)	54.1

[a] Calculational details provided in section VI. [b] See Table VI, footnote *c*. [c] The total energy of the H atom within the DZ (and DZP) basis is −0.499 28 hartree. [d] CCCI ≡ RCI*[SD_{Ru-H} + S_{val}].

increasing level of electron correlation. The CCCI results listed in each table correspond to the values shown in Figure 7.

Table V lists the adiabatic Ru=C bond energies in ClRuH(CH_2) (**1a**), dissociating the optimized geometry of **1a** (Table II) to the optimum structure for the ^{3}A′ state of ClRuH [R_e(Ru–H) = 1.64 Å, R_e(Ru–Cl) = 2.38 Å, and θ_e(Cl–Ru–H) = 104.8°] and the equilibrium geometry of CH_2 ($^3B_1$) [R_e(C–H) = 1.08 Å and θ_e(H–C–H) = 133°]. We see that HF theory predicts an Ru=C bond strength too low by 71 kcal/mol! The final CCCI value, D_e(ClHRu=CH_2) = 84.7 kcal/mol, should be representative of Ru=CH_2 bond energies in coordinatively saturated systems.[7,28] Similar calculations on ethylene yield D_e(H_2C=CH_2) = 174.1 kcal/mol,[10] which is 4.9 ± 2.5 kcal/mol below the best experimental value. We expect a similar error for Ru=C and hence predict D_e(ClHRu=CH_2) = 89.6 ± 2.5 kcal/mol, based on the correlation error inherent to the CCCI description of double bonds.

Table VIII. Adiabatic Ru-CH_3 Bond Energies (D_e) in ^{1}A′ ClRu-CH_3 (kcal/mol)

calculation[a]	basis set[b]	total energies (hartrees) ^{1}A′ ClRuCH$_3$	^{2}A′ ClRu	^{2}A$_2$″ CH$_3$	D_e(Ru–C)
HF	VDZ	−4936.425 11 (1/1)	−4896.857 40 (1/1)	−39.549 46 (1/1)	11.5
GVB-PP	VDZ	−4936.474 22 (8/8)	−4896.861 88 (2/2)	−39.564 71 (2/2)	29.9
RCI	VDZ	−4936.480 19 (27/37)	−4896.861 88 (3/4)	−39.566 20 (3/4)	32.7
RCI*SD$_{Ru-C}$	VDZ	−4936.486 72 (1843/3191)	−4896.861 97 (32/42)	−39.569 43 (6/8)	34.7
CCCI[c]	VDZ	−4936.528 00 (3457/7113)	−4896.862 58 (76/152)	−39.581 20 (42/104)	52.9
HF	VDZD	−4936.436 68 (1/1)	−4896.857 40 (1/1)	−39.560 32 (1/1)	11.9
GVB-PP	VDZD	−4936.486 92 (8/8)	−4896.861 88 (2/2)	−39.575 49 (2/2)	31.1
RCI	VDZD	−4936.493 12 (27/37)	−4896.861 88 (3/4)	−39.576 77 (3/4)	34.2
RCI*SD$_{Ru-C}$	VDZD	−4936.503 39 (2545/4462)	−4896.861 97 (32/42)	−39.587 37 (25/44)	33.9
CCCI	VDZD	−4936.545 80 (4510/9272)	−4896.862 58 (76/152)	−39.596 67 (58/143)	54.3

[a] Calculations discussed in detail in section VI. [b] See Table V, footnote *b*. [c] CCCI ≡ RCI*[SD$_{Ru-C}$ + S$_{val}$].

Table VI displays the adiabatic singlet–triplet splittings [$\Delta E_{ST} = E(^1A') - E(^3A'')$] for ClRuH. The equilibrium geometry of the ^{3}A″ state of ClRuH is listed above and the equilibrium structure of the ^{1}A′ state of ClRuH is found to be R_e(Ru–H) = 1.59 Å, R_e(Ru–Cl) = 2.35 Å, and θ_e(Cl–Ru–H) = 101.3°. ΔE_{ST} changes only slightly among all the levels listed, with the final CCCI result of 16.9 kcal/mol the same for polarized and unpolarized basis sets.

Table VII presents adiabatic Ru–H bond energies for ClRuH (^{1}A′), using the equilibrium bond distance of 2.39 Å for RuCl (^{2}A′). At the highest level of correlation (CCCI) and basis (VDZP), we find D_e(ClRu–H) = 54.1 kcal/mol. Since the model complex is low spin and does not suffer exchange losses during bond formation, this value should be representative of coordinatively saturated Ru–H bond energies.[28] Furthermore, D_e(ClRu–H, ^{1}A′) should be higher than the bond energy in the coordinatively unsaturated complex Ru^+–H by 14.6 kcal/mol,[28] leading to a predicted bond energy for $D_e(Ru^+–H)$ = 39.5 kcal/mol, in excellent agreement with the experimental value of 41 ± 3 kcal/mol[29] and in reasonable agreement with a theoretical value of 34.5 kcal/mol.[30]

Adiabatic bond energies for ClRu–CH_3 (^{1}A′) (**2**) are shown in Table VIII, using the equilibrium geometry for **2** shown in the last column of Table IV, the optimum bond length for ClRu (^{2}A′) of 2.39 Å, and the experimental geometry for CH_3 (^{2}A″) of R_e(C–H) = 1.079 Å and θ_e(H–C–H) = 120.0°.[31] At the CCCI level, D_e(ClRu–CH_3) = 54.3 kcal/mol within the VDZD basis, essentially identical with the Ru–H bond energy. While this result is contrary to the trends in coordinatively saturated complexes, where M–CH_3 bond strengths are thought to be weaker than the corresponding M–H bond energies by 10–15 kcal/mol,[32] the result is in excellent agreement with the experimental Ru^+–CH_3 bond energy of 54 ± 5 kcal/mol. This agreement is probably due to a cancellation of two effects: (i) the differential exchange loss incurred when bonds are formed in a saturated versus an unsaturated complex[7,28] (leading to a bond *weakening* of ~15 kcal/mol going from saturated to unsaturated Ru complexes) and (ii) the extra stabilization of $RuCH_3^+$ due to the polarizability of the methyl ligand (resulting in a bond *strengthening*, relative to a neutral system, of ~15 kcal/mol).[29] Thus, the Ru–CH_3 bond energy predicted here should be representative

Table IX. Adiabatic CH_2–H Bond Energies (D_e) in $^2A_2''$ CH_3 (kcal/mol)[a]

calculation	basis set[b]	total energies (hartrees)[c] ^{2}A$_2$″ CH$_3$	^{3}B$_1$ CH$_2$	D_e(CH$_2$–H)
HF	VDZ	−39.549 46 (1/1)	−38.913 49 (1/1)	85.8
GVB-PP	VDZ	−39.564 71 (2/2)	−38.913 49 (1/1)	95.3
RCI	VDZ	−39.566 20 (3/4)	−38.913 49 (1/1)	96.3
RCI*SD$_{C-H}$	VDZ	−39.570 66 (36/60)	−38.913 49 (1/1)	99.1
CCCI[d]	VDZ	−39.584 87 (65/140)	−38.920 67 (14/28)	103.5
HF	VDZD	−39.560 32 (1/1)	−38.922 54 (1/1)	86.9
GVB-PP	VDZD	−39.575 49 (2/2)	−38.922 54 (1/1)	96.4
RCI	VDZD	−39.576 77 (3/4)	−38.922 54 (1/1)	97.2
RCI*SD$_{C-H}$	VDZD	−39.587 43 (61/104)	−38.922 54 (1/1)	103.9
CCCI	VDZD	−39.605 48 (102/215)	−38.934 25 (20/40)	107.9
HF	VDZDP	−39.562 82 (1/1)	−38.922 54 (1/1)	88.5
GVB-PP	VDZDP	−39.577 50 (2/2)	−38.922 54 (1/1)	97.7
RCI	VDZDP	−39.578 74 (3/4)	−38.922 54 (1/1)	98.5
RCI*SD$_{C-H}$	VDZDP	−39.594 98 (80/138)	−38.922 54 (1/1)	108.7
CCCI	VDZDP	−39.613 40 (130/271)	−38.934 25 (20/40)	112.9
expt[e]				115.8 ± 1.4

[a] Calculational details provided in section VI. [b] VDZ and VDZD: see Table V, footnote *b*. VDZDP: one set of unscaled p-polarization functions for the hydrogen atom involved in the breaking C–H bond was added to the VDZD basis. [c] The total energy of the H atom within the DZ (and DZP) basis is −0.499 28 hartree. [d] CCCI ≡ RCI*[SD$_{C-H}$ + S$_{val}$]. [e] Reference 33.

(28) The difference in Ru–H bond energies in singlet ClRuH and triplet Ru^+–H may be attributed to differential exchange loss suffered by Ru when the Ru–H bond is formed. Here the difference amounts to one d-d exchange term, $K_{dd}(Ru^+)$ = 14.6 kcal/mol. (Carter, E. A.; Goddard, W. A., III *J. Phys. Chem.* submitted for publication).

(29) Mandich, M. L.; Halle, L. F.; Beauchamp, J. L. *J. Am. Chem. Soc.* **1984**, *106*, 4403.

(30) Schilling, J. B.; Goddard, W. A., III; Beauchamp, J. L. *J. Am. Chem. Soc.* **1987**, *109*, 5565.

(31) Herzberg, G. *Proc. R. Soc., London, Ser. A* **1961**, *A262*, 291.

(32) Martinho Simões, J. A.; Beauchamp, J. L. *Chem. Rev.*, submitted for publication.

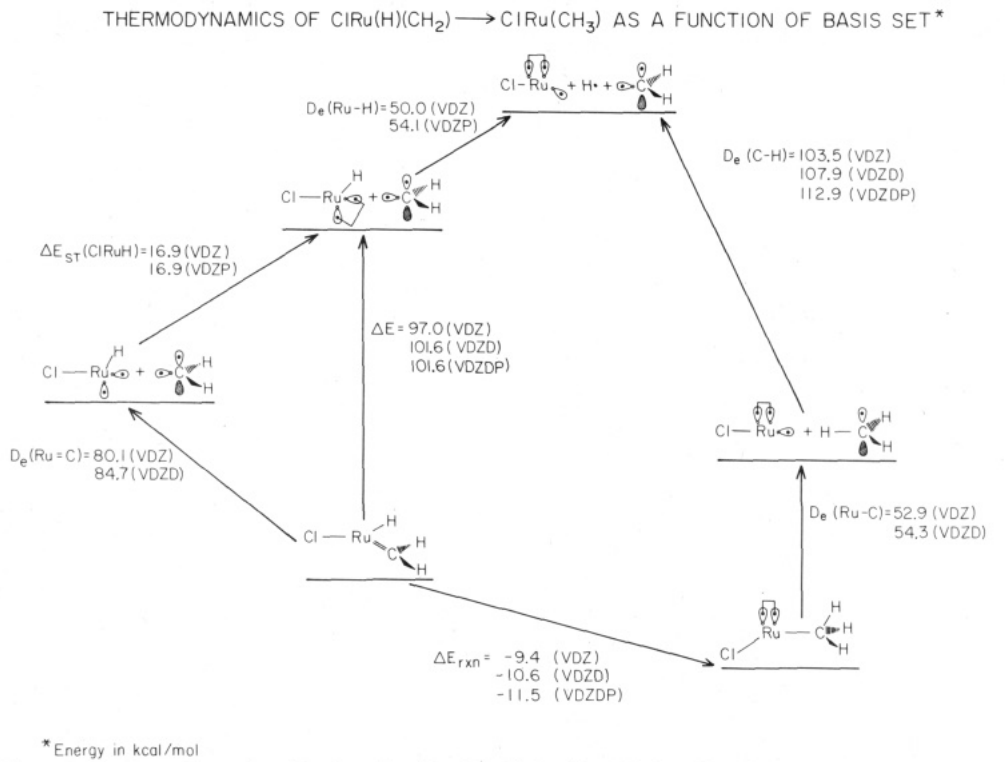

Figure 7. The thermodynamic cycle used to derive ΔE_{rxn} (kcal/mol) for (7). The bond and excitation energies shown are from CCCI calculations (sections IV and VI) using the VDZ, VDZD, and VDZDP basis sets (Table V, footnote *b*, and Table VI, footnote *c*; section VI). The predicted exothermicities (ΔE_{rxn}) are shown at the bottom.

Table X. Direct Calculations of the Insertion Activation Barrier (E_a) and Exothermicity (ΔE_{rxn}) within Both VDZ and VDZDP Bases as a Function of Electron Correlation (kcal/mol)[a]

	total energies (hartrees)									
	VDZ basis[b]			VDZDP basis[c]			E_a		ΔE_{rxn}	
calculation	**1a**	TS[d]	**2**	**1a**	TS	**2**	VDZ	VDZDP	VDZ	VDZDP
RCI(3/6)[e]	−4936.463 72	−4936.441 19	−4936.480 20	−4936.474 94	−4936.457 13	−4936.495 08	14.1	11.2	−10.3	−12.6
RCI(3/6)*SD[f]	−4936.487 31	−4936.470 86	−4936.497 52	−4936.511 91	−4936.497 18	−4936.527 11	10.3	9.2	−6.4	−9.5
CCCI[g]	−4936.517 29	−4936.495 42	−4936.531 67	−4936.545 21	−4936.525 10	−4936.563 73	13.7	12.6	−9.0	−11.6
best estimate[h]								10.9 ± 1.7		−10.6 ± 1.0

[a] Details of the calculations are provided in section VI. [b] VDZ: see Table V, footnote *b*. [c] VDZDP: VDZ + one set of d-polarization functions on C (ζ = 0.64) and one set of unscaled p-polarization functions on the migrating H. [d] TS ≡ geometry at transition state where θ(H–Ru–C)† = 50.0° (section III). [e] 27 spatial configurations/37 spin eigenfunctions. [f] RCI(3/6)*SD ≡ RCI(3/6)*[$SD_{Ru-Hbond/C-Hbond}$ + $SD_{Ru-C\sigma bond}$ + $SD_{Ru-C\pi bond/Ru4dlonepair}$]. VDZ: 5475 spatial configurations/9499 spin eigenfunctions. VDZDP: 9084 spatial configurations/16048 spin eigenfunctions. [g] CCCI ≡ RCI(3/6)*[$SD_{Ru-Hbond/C-Hbond}$ + $SD_{Ru-C\sigma bond}$ + $SD_{Ru-C\pi bond/Ru4dlonepair}$ + S_{val}]. VDZ: 6501 spatial configurations/12 337 spin eigenfunctions; VDZDP: 10 488 spatial configurations/19 950 spin eigenfunctions. [h] Based on the average of the RCI(3/6)*SD and CCCI values using the VDZDP basis.

of coordinatively saturated (or low spin unsaturated) $RuCH_3$ bonds.[28]

The adiabatic C–H bond energies in CH_3 are shown in Table IX for three different basis sets and five levels of theory. The bond strengths increase dramatically upon the inclusion of electron correlation. The CCCI value (within the VDZDP basis) for $D_e(CH_2–H)$ is 112.9 kcal/mol, in good agreement with the experimental value [$D_e^{exptl}(CH_2–H)$ = 115.8 ± 1.4 kcal/mol[33]].

The exothermicities calculated by using the CCCI values from Tables V–IX are shown at the bottom of Figure 7 for three different basis sets. The VDZ basis set result of ΔE_{rxn} = −9.4 kcal/mol is in good agreement with the GVBCI-MCSCF result of −7.1 kcal/mol (Table III), suggesting that the dominant correlations important in the reaction are already included at the valence level (GVBCI). Considering the number of calculations required to complete the thermodynamic cycle of Figure 7, the agreement is excellent. Increasing the basis as well as the electron correlational level serves to increase the exothermicity slightly, to a final value of ΔE_{rxn} = −11.5 kcal/mol.

Figure 7 yields thermodynamic estimates for the overall exothermicity of (7) but yields no information about the height of the barrier (kinetics). For an independent prediction of the barrier height as a function of electron correlation, we carried out CCCI calculations (section VI) on the reactant **1a**, the transition state geometry [θ(H–Ru–C)† = 50°], and the product **2**, for both the VDZ and the VDZDP basis sets. The results are shown in Table X, where we see an across-the-board decrease in the activation energy and an increase in the exothermicity going from VDZ to VDZDP bases. A slight overall decrease in the activation energy and the exothermicity is seen going from the valence level CI [RCI(3/6)] to the higher order CI's. Our best estimates for E_a and ΔE_{rxn} are obtained simply

(33) (a) The total energies for CH_2 differ slightly from the values listed in Table V, due to one change in the basis set between complex 1 (where the 3s combination of the 3d-polarization functions on carbon was included in the calculation) and CH_3 [where the 3s combination was omitted[10a]); (b) the experimental D_e was derived from $\Delta H_f°_0$ in: *JANAF Thermochemical Tables*, **1971**, *NSRDS-NBS 37* and supplements to JANAF in: *J. Phys. Chem. Ref. Data* **1975**, *4*, 1; **1982**, *11*, 695, with zero point energy corrections from: Jacox, M. E. *J. Phys. Chem. Ref. Data* **1984**, *13*, 945 for CH_3 and from: Bunker, P. R.; Jensen, P.; Kraemer, W. P.; Beardsworth, R. *J. Chem. Phys.* **1986**, *85*, 3724 for CH_2.

by averaging the results from the two higher order CI's within the extended basis (VDZDP).

Thus we have used two different techniques to arrive at independent estimates of the energetics of the migratory insertion reaction of CH_2 into an adjacent Ru–H bond. The exothermicities and activation barriers are in close agreement from all three methods [ΔE_{rxn} = −7.1 (GVBCI-MCSCF), −11.5 (Figure 7), and −10.6 ± 1.0 (Table X) kcal/mol; E_a = 11.5 (GVBCI-MCSCF) and 10.9 ± 1.7 (Table X) kcal/mol], lending credence to the reliability of these methods for the prediction of energetics in organometallic systems.

V. Discussion and Summary

The migratory insertion of a terminal CH_2 ligand into an adjacent ruthenium–hydrogen bond is predicted to be exothermic by 10.5 ± 1.0 kcal/mol and to proceed with a small barrier (10.9 ± 1.7 kcal/mol), with a preferred orientation of the CH_2 ligand *perpendicular* to the bond into which it will insert. We have thus demonstrated the feasibility of the FT chain initiation step (1) to occur at one metal center. Group VIII (8–10) metals are by far the most active for FT synthesis; perhaps another reason for their higher activity (aside from their ability to readily dissociate carbon monoxide) is this low barrier for chain initiation. Early metals are not good catalysts for FT synthesis, presumably because the M=CH_2 bond strength is too strong, leading to an endothermic process.[8b,34]

The analogous insertion of CH_2 into an adjacent Ru–CH_3 bond (eq 11) can be predicted by using the bond energies and excitation energies in Figure 7, along with an estimate for the C–C bond strength of ethyl radical. The

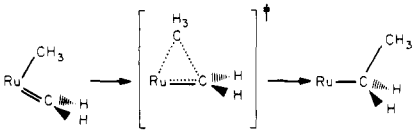

(11)

methyl migration thermodynamic cycle will be identical to that of Figure 7, except for two steps: (i) instead of the Ru–H bond in ClRuH ($^1A'$) breaking, we now break an Ru–CH_3 bond in the $^1A'$ state of $ClRuCH_3$ [D_e(Ru–CH_3) = 54.3 kcal/mol; see Figure 7] and (ii) instead of breaking the C–H bond of methyl radical, we break the C–C bond of ethyl radical [D_e(H_3C–$CH_2^\bullet$) = 105.8 ± 3.4 kcal/mol[35]]. We assume here that the singlet–triplet splittings of ClRuH and $ClRuCH_3$ are the same (we expect that the singlet–triplet splitting is more a function of the metal than of the ancillary ligands) and that D_e(Ru–Et) is the same as D_e(Ru–Me). Given these two assumptions, we find that the insertion of CH_2 into an Ru–CH_3 bond is downhill by 4.2 ± 3.4 kcal/mol. This insertion is less exothermic than for the insertion into an Ru–H bond because the incipient C–C bond is 7.1 ± 3.4 kcal/mol weaker than the incipient C–H bond. Furthermore, steric factors would suggest that D_e(Ru–Et) should be less than D_e(Ru–Me), which would lead to an even less exothermic reaction (perhaps even endothermic). A higher barrier is expected for methyl migration over hydrogen migration due partly to the smaller exothermicity (the Hammond postulate) and partly to the essential reorientation of the methyl group (with its directed sp^3 hybrid orbital) during the migration from Ru to CH_2 (H has no such reorientation problems due to the spherical nature of its 1s orbital).[36] Consistent with this expectation, Bercaw et al. found the barrier for CH_3 to be higher than for H by 14 kcal/mol for migration to Ta=CH_2.[8b] In addition, Low and Goddard showed that for reductive elimination from Pd (eq 12) there is essen-

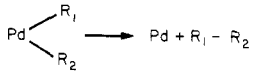

(12)

tially no barrier if R_1 = R_2 = H, a barrier of ~10 kcal/mol if one R = H, and ~20 kcal/mol if both R = CH_3.[36] Thus we estimate the barrier for alkyl migration to Ru=CH_2 to be ~20 kcal/mol. As a result, chain propagation should generally be the rate-determining step in FT synthesis. Indeed, for some group VIII (8–10) metals (e.g., Ni), the chain propagation step is so unfavorable that the only product of FT synthesis is methane.[37]

The present work yields the following conclusions: (i) methylidene insertions into metal–hydrogen bonds should be facile, with low barriers (~10.9 kcal/mol) and moderate exothermicities (~10.5 kcal/mol) for late transition metals (since the M=C double bonds are relatively weak compared to those of early metals) *only if the orientation of the CH_2 ligand is perpendicular to bond into which it will insert*; (ii) the reverse reaction of α-hydride elimination is predicted to be uphill by ~21 kcal/mol, consistent with the lack of evidence for α-hydride eliminations among late transition metals; (iii) the analogous insertion of CH_2 into an Ru–CH_3 bond is predicted to be less exothermic (ΔE_{rxn} ≈ −4 kcal/mol) than for insertion into Ru–H, due to the weaker incipient bond formed (C–C versus C–H). The activation barrier should be higher by ~10–15 kcal/mol due to the lower exothermicity and the reorientation of the sp^3 hybrid on CH_3 during its migration (E_a ≈ 20–25 kcal/mol); and (iv) the implications for FT synthesis from (i) and (iii) are that chain initiation should proceed readily with a low barrier while chain propagation is predicted to be the rate-determining step for late transition metals. However, since polymethylene is the only product observed on heterogeneous Ru catalysts, insertion of CH_2 into Ru–R must have a *lower* barrier than into Ru–H, which suggests that the Ru–CH_3 bond energy on a Ru surface is ~10–15 kcal/mol weaker than the Ru–H surface bond energy (leading to a smaller barrier for CH_2 insertion into Ru–R than for Ru–H).

VI. Calculational Details

All of the electrons of Ru, C, and H were treated explicitly with valence double-ζ (VDZ) basis sets. The Cl atom was described by using the SHC effective potential to represent the core electrons,[38a] and the double-ζ basis was contracted to minimal basis from calculations on $TiCl_4$.[38b] The VDZ basis consisted of a valence double-ζ basis for Ru,[7,39] the Dunning valence double-ζ contrac-

(34) Carter, E. A.; Goddard, W. A., III *J. Am. Chem. Soc.* **1986**, *108*, 4746.

(35) D_e(H_3C–$CH_2^\bullet$) was estimated from D_{298}(H_3C–$CH_2^\bullet$) = 101.3 ± 2.2 kcal/mol [$\Delta H_f°_{298}$ was taken from JANAF (ref 33b) for: CH_2 (92.35 ± 1 kcal/mol) and $CH_3^\bullet$ (34.82 ± 0.2 kcal/mol) and $\Delta H_f°_{298}$ for $C_2H_5^\bullet$ (25.9 ± 1 kcal/mol) was taken from: McMillen, D. F.; Golden, D. M. *Annu. Rev. Phys. Chem.* **1982**, *33*, 493]. Temperature corrections for the heat capacity changes going to T = 0 K were taken equal to $4R\Delta T$ = 2.4 kcal/mol, leading to D_0(H_3C–$CH_2^\bullet$) = 98.9 ± 2.2 kcal/mol. Finally, D_e(H_3C–$CH_2^\bullet$) = 105.8 ± 3.4 was obtained from zero point energy corrections to D_0(ΔZPE = 6.9 ± 1.2 kcal/mol from ref 10a and references therein).

(36) Low, J. J.; Goddard, W. A., III *Organometallics* **1986**, *5*, 609.

(37) Kelley, R. D.; Goodman, D. W. In *The Chemical Physics of Solid Surfaces and Heterogeneous Catalysis*; Elsevier: Amsterdam, 1982; Vol. 4, pp 427–453.

(38) (a) Rappé, A. K.; Smedley, T. A.; Goddard, W. A., III *J. Phys. Chem.* **1981**, *85*, 1662. (b) Rappé, A. K.; Goddard, W. A., III, unpublished results.

(39) (a) Rappé, A. K.; Goddard, W. A., III, to be submitted for publication. This basis set was optimized for the d^n configuration of the metal as discussed in: Rappé, A. K.; Smedley, T. A.; Goddard, W. A., III *J. Phys. Chem.* **1981**, *85*, 2607.

tions[40] of the Huzinaga (9s5p) and (4s) primitive Gaussian bases for carbon and hydrogen[41] (exponents for H scaled by 1.2). The VDZP basis added one set of unscaled 2p-polarization functions for the migrating hydrogen ($\zeta^p = 1.0$) to the VDZ basis. The VDZD basis added one set of carbon 3d-polarization functions ($\zeta^d = 0.64$) to the VDZ basis. The VDZDP basis added the two polarization functions above to the VDZ basis.

The geometries of **1a**, **1b**, and **6a** were optimized at the GVB-RCI level [RCI(3/6) for **1a** and **1b**; RCI(1/2) for **6a**, leaving the Ru–Cl bond at the HF level]. The RCI (restricted configuration interaction) starts from the GVB-PP wave function (generalized valence bond with perfect-pairing restriction) in which each correlated bond pair (Ru–H, Ru–C σ, Ru–C π) is described with two orbitals, so that each electron involved in the insertion process has its own orbital. All other electron pairs were left uncorrelated (but calculated self-consistently). The GVB-RCI wave function allows all configurations arising from the three possible occupations of two electrons in two orbitals for each GVB bond pair. [The rotational barrier in **1** was calculated at the GVB-RCI(3/6) level.] The geometries of **2**, the $^1A'$ state of ClRuH, and the $^2A'$ state of RuCl were optimized by using Hartree–Fock (HF) gradient techniques.

The reaction pathway was followed at the HF, the GVB-PP(3/6), the GVB-RCI(3/6), the GVBCI(3/6), and the GVBCI(3/6)-MCSCF levels. The GVBCI(3/6) allows a full CI within the six "active" orbitals (e.g., the Ru–C bond pairs and the Ru–H bond pair), while the GVBCI-(3/6)-MCSCF self-consistently optimizes the orbitals for the GVBCI(3/6) wave function.

The bond and excitation energies of the various species in Tables V–IX were calculated at the HF, GVB-PP, GVB-RCI, and higher order CI levels now described: (i) RCI*S_{val} allows all single excitations from all valence orbitals (except Cl) to all virtual (unoccupied) orbitals from the RCI reference configurations; (ii) RCI*[SD_{pair1} + SD_{pair2} + ...] allows all single and double excitations to all virtuals from pair 1, pair 2, etc. (but *not* simultaneously) from the RCI reference configurations; (iii) CCCI adds the configurations of (ii) to the configurations of (i), allowing for full correlation of the changing bonds (RCI*SD) along with orbital shape readjustments for the other valence orbitals (RCI*S_{val}).[10]

Acknowledgment. This work was supported by the National Science Foundation (Grant No. CHE83-18041). In addition, it was partially supported by the Shell Companies Foundation and Shell Development Corp. E.A.C. acknowledges a National Science Foundation predoctoral fellowship (1982–1985), a research grant award from the International Precious Metals Institute and Gemini Industries (1985–1986), and a SOHIO fellowship in catalysis (1986–1987).

Registry No. 1, 106252-75-9; 2, 106252-76-0; ClRuH, 112022-68-1; CO, 630-08-0; Ru, 7440-18-8.

(40) Dunning, T. H., Jr. *J. Chem. Phys.* **1970**, *53*, 2823.
(41) Huzinaga, S. *J. Chem. Phys.* **1965**, *42*, 1293.

Ruthenium, Rhodium, and Iridium Complexes of π-Bound Thiophene and Benzo[*b*]thiophenes: Models for Thiophene Binding to HDS Catalysts

Sara C. Huckett, Lance L. Miller, Robert A. Jacobson, and Robert J. Angelici*

Department of Chemistry and Ames Laboratory,[1] Iowa State University, Ames Iowa 50011

Received July 11, 1987

Ru, Rh, and Ir complexes of π-bound thiophene (T) and benzo[*b*]thiophenes (BTs), $(\eta\text{-}C_5H_5)Ru(BT)^+$, $(\eta\text{-}C_5Me_5)M(BT)^{2+}$, and $(\eta\text{-}C_5Me_2)M(T)^{2+}$ (M = Rh, Ir), which serve as models for the adsorption of thiophenes on hydrodesulfurization (HDS) catalysts, have been synthesized. The Rh and Ir compounds are the first dicationic transition metal complexes of either T or BTs. The BT ligands are bound to the transition metal centers via the benzene ring. The first X-ray structural characterization of a BT complex, $[(\eta\text{-}C_5H_5)Ru(\eta^6\text{-}BT)]BF_4$ (**1**), is reported.

The process of catalytic hydrodesulfurization (HDS) is performed industrially on a very large scale in order to remove sulfur from crude oils.[2] Typically, sulfided-cobalt-promoted molybdenum catalysts are used.[3] The mechanism of desulfurization has been investigated intensively, but in spite of this effort key aspects of HDS such as binding of sulfur-containing hydrocarbons to the catalyst surface as well as important steps in the HDS process are not well-understood.[4]

Thiophene (T) has frequently been used as a representative sulfur-containing compound in mechanistic investigations involving heterogeneous reactor studies.[5] It

(1) Ames Laboratory is operated for the U.S. Department of Energy by Iowa State University under Contract No. W-7405-Eng-82. This research was supported by the Office of Basic Energy Sciences, Chemical Sciences and Materials Sciences Divisions.
(2) (a) Houalla, M.; Nag, N. K.; Sapre, A. V.; Broderick, D. H.; Gates, B. C. *AIChE J.* **1978**, *24*, 1015. (b) Houalla, M.; Broderick, D. H.; Sapre, A. V.; Nag, N. K.; de Beer, V. H. J.; Gates, B. C.; Kwart, H. *J. Catal.* **1980**, *61*, 523.
(3) Gates, C. B.; Katzer, J. R.; Schuit, G. C. A. *Chemistry of Catalytic Processes*; McGraw-Hill: New York, 1979; p 393.
(4) (a) Massoth, F. E.; Murali Dhar, G. *Proceedings, Climax 4th International Conference on the Chemistry and Uses of Mo*; Barry, P. C., Mitchell, P. C. H., Eds.; Climax Molybdenum Co.: Ann Arbor, MI, 1985; p 343. (b) Zdrazil, M. *Appl. Catal.* **1982**, *4*, 107.
(5) (a) Smith, G. V.; Hinckley, C. C.; Behbahany, F. *J. Catal.* **1973**, *30*, 218. (b) Schuit, G. C. A.; Gates, B. C. *AIChE J.* **1973**, *19*, 417. (c) Pazos, J. M.; Andrév, P. *Can. J. Chem.* **1980**, *58*, 479.

0276-7333/88/2307-0686$01.50/0